Dalton Transactions

Cite this: *Dalton Trans.*, 2011, **40**, 2725

www.rsc.org/dalton

PAPER

Varying spin state composition by the choice of capping ligand in a family of molecular chains: detailed analysis of magnetic properties of chromium(III) horseshoes†

Michael L. Baker,*[a,b] Alberto Bianchi,[c] Stefano Carretta,[c] David Collison,[a] Rebecca J. Docherty,[a] Eric J. L. Mclnnes,[a] Andrew McRobbie,[a] Christopher A. Muryn,[a] Hannu Mutka,[b] Stergios Piligkos,[e] Marzio Rancan,[a] Paolo Santini,[c] Grigore A. Timco,[a] Philip L. W. Tregenna-Piggott,‡[d] Floriana Tuna,[a] Hans U. Güdel[d] and Richard E. P. Winpenny*[a,f]

Received 16th September 2010, Accepted 23rd December 2010
DOI: 10.1039/c0dt01243b

We report a detailed physical analysis on a family of isolated, antiferro-magnetically (AF) coupled, chromium(III) finite chains, of general formula $(Cr(RCO_2)_2F)_n$ where the chain length $n = 6$ or 7. Additionally, the chains are capped with a selection of possible terminating ligands, including hfac (= l,l,l,5,5,5-hexafluoropentane-2,4-dionate(l-)), acac (= pentane-2,4-dionate(l-)) or $(F)_3$. Measurements by inelastic neutron scattering (INS), magnetometery and electron paramagnetic resonance (EPR) spectroscopy have been used to study how the electronic properties are affected by n and capping ligand type. These comparisons allowed the subtle electronic effects the choice of capping ligand makes for odd member spin 3/2 ground state and even membered spin 0 ground state chains to be investigated. For this investigation full characterisation of physical properties have been performed with spin Hamiltonian parameterisation, including the determination of Heisenberg exchange coupling constants and single ion axial and rhombic anisotropy. We reveal how the quantum spin energy levels of odd or even membered chains can be modified by the type of capping ligand terminating the chain. Choice of capping ligands enables Cr–Cr exchange coupling to be adjusted by 0, 4 or 24%, relative to Cr–Cr exchange coupling within the body of the chain, by the substitution of hfac, acac or $(F)_3$ capping ligands to the ends of the chain, respectively. The manipulation of quantum spin levels *via* ligands which play no role in super-exchange, is of general interest to the practise of spin Hamilton modelling, where such second order effects are generally not considered of relevance to magnetic properties.

1 Introduction

The analytic study of infinite AF spin chains can be traced back to the 1950's when spin wave theory for ferromagnetic systems was extended to describe the approximate quantum theory of AF systems.[1] The use of spin wave theory has proved to be a fundamentally successful model in solid state magnetism. The study of low dimensional magnetic systems has yielded new phenomena including exotic physics such as high temperature super conductivity.[2] More recently finite spin chains have drawn particular interest, where impurities or engineered atomic structure has enabled the study of one dimensional spin segments.[3] When dealing with a finite number of spin centers an exact quantum mechanical approach can be adopted, leading to a discrete number of energy levels. Coordination chemistry provides an alternative means to obtain finite spin chains. Here we rely on this molecular route to obtain such systems. Work on clusters composed of Cr^{3+} has given a family of AF spin 3/2 chains,

[a]*School of Chemistry, The University of Manchester, Oxford Road, Manchester, UK M13 9PL, United Kingdom*
[b]*Institut Laue-Langevin, BP 156, 6 rue Jules Horowitz, 38042, Grenoble Cedex 9, France. E-mail: baker@ill.fr*
[c]*Dipartimento di Fisica, Universit di Parma, 1-43100, Parma, Italy*
[d]*Department of Chemistry and Biochemistry, University of Bern, Freiestrasse 3, 3000, Bern 9, Switzerland*
[e]*Department of Chemistry, University of Copenhagen Universitetsparken 5, 2100, Copenhagen, Denmark*
[f]*Photon Science Institute, University of Manchester, Oxford Road, Manchester, UK M13 9PL*

† Electronic supplementary information (ESI) available: INS spectra with simulations of **4** measured 9.0 and 3.2 Å. Q dependencies of several magnetic transitions for **4** and **5**. INS spectra at 3.2 and 6.5 Å with susceptibility results and simulations of **1** and **6**. Susceptibility results with simulations of **2**. CCDC reference number (for **6**) 790095 . For ESI and crystallographic data in CIF or other electronic format see DOI: 10.1039/c0dt01243b

‡ Dedicated to the memory of Dr Philip L. W. Tregenna-Piggott.

including examples with an odd or even number of spin centers, where molecular chains of Cr^{3+} are magnetically isolated.

In 2008 we reported detailed characterisation of two dimeric spin chains.[4] These chains form the shape of a horseshoe, where the body of individual chains arc around a templating and charge balancing cation, which bridges fluoride atoms. Three fluoride ligands terminate each chain. Terminal fluorides hydrogen bond *via* a protonated amine, di-iso-propylamine or diethylamine, to a neighbouring equivalent chain. Two dimeric chain variants with six or seven Cr^{3+} ions were investigated, $[([nPr_2NH_2]_3[Cr_6F_{11}(O_2CCMe_3)_{10}])_2]$ **1** (Fig. 1) and $[([iPr_2NH_2]_3[Cr_7F_{12}(O_2CCMe_3)_{12}])_2]$ **2** respectively. The horseshoe units were shown to be magnetically isolated from neighbouring chains. The horseshoe unit can be considered an AF chain segment, comparable to the previously reported and well characterised homometallic ring,[5] $[(CrF(O_2CCMe_3)_2)_8]$ **3**, with one or two Cr^{3+} ions removed. Conversely magnetic characterisation of dimeric chains showed the Cr–Cr exchange coupling and local Cr^{3+} ion anisotropy to differ significantly from that of the Cr_8 ring, **3**.

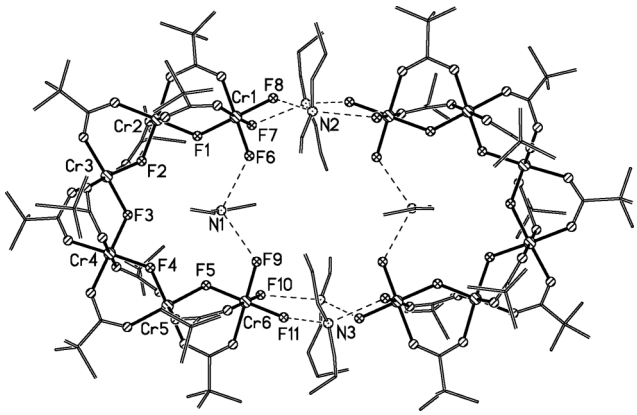

Fig. 1 The structure of Cr_6 dimer chains (**1**) terminated with $(F)_3$ H-bonded to two protonated di-iso-propylamines.

Further synthetic work allows the two segments of the dimeric chain to be structurally isolated. The structure of the single Cr_6 and Cr_7 are very similar to the respective dimer versions. These fully isolated versions are available with two possible terminal ligands, hfac (l,l,l,5,5,5-hexafluoropentane-2,4-dionate(l-)) or acac (pentane-2,4-dionate(l-)), which cap the ends of the chain. Fig. 2 shows the structures of isolated Cr_6 chains with hfac and acac capping ligands.

This paper reports the characterisation of isolated finite chains $[(iPr_2NH_2)Cr_7F_8(O_2CtBu)_{12}(hfac)_2]$ **4**, $[(Et_2NH_2)(Cr_6F_7(O_2CtBu)_{10}(hfac)_2)]$ **5** and $[(Et_2NH_2)(Cr_6F_7(O_2CtBu)_{10}(acac)_2)]$ **6**, and makes quantitative comparisons between the physical properties of these compounds relative to **1**, **2** and **3**. INS, magnetic and EPR techniques have been used collectively leading to accurate determination of inter-chromium exchange coupling and single ion zero field splitting (ZFS) within chain segments.

2 Experimental

2.1 Preparation of compounds

All reagents, metal salts and ligands were used as obtained from Aldrich. Analytical data were obtained by the microanalytical service of the University of Manchester. Complexes **1** and **2** were prepared by a variation of the literature method.[4] Complex **5** was prepared as described in ref. 6.

1. Pivalic acid (16.0 g, 157 mmol), diethylamine (1.64 g, 22 mmol) and $CrF_3{\cdot}4H_2O$ (5.0 g, 28 mmol) were stirred together at 140 °C for 15 h in an open Teflon flask. The mixture was then cooled to room temperature and acetone (50 mL) was added and the mixture stirred for 5 h. The resulting solid was collected by filtration, washed with acetone and dried in air. The solid was then extracted with diethyl ether (75 mL), the solution was filtered and MeCN (30 mL) added. The solution was stirred for 30 min. and then the green microcrystalline precipitate was collected by filtration, washed with a large quantity of MeCN and then acetone, and dried in air. Yield: 6.4 g (78.4%). Elemental analysis calcd (%) for $C_{124}H_{256}Cr_{12}F_{22}N_60_{42}$: Cr 17.60, C 42.01, H 7.28, N 2.37; found: Cr 17.32, C 42.27, H 7.52, N 2.42.

2. Pivalic acid (16.0 g, 157 mmol), di-*iso*-propylamine (2.0 g, 22 mmol) and $CrF_3{\cdot}4H_2O$ (5.0 g, 28 mmol) were stirred together at 140 °C for 18 h in an open Teflon flask. The resulting viscous solid was heated at 100 °C under a N_2 flow to remove unreacted

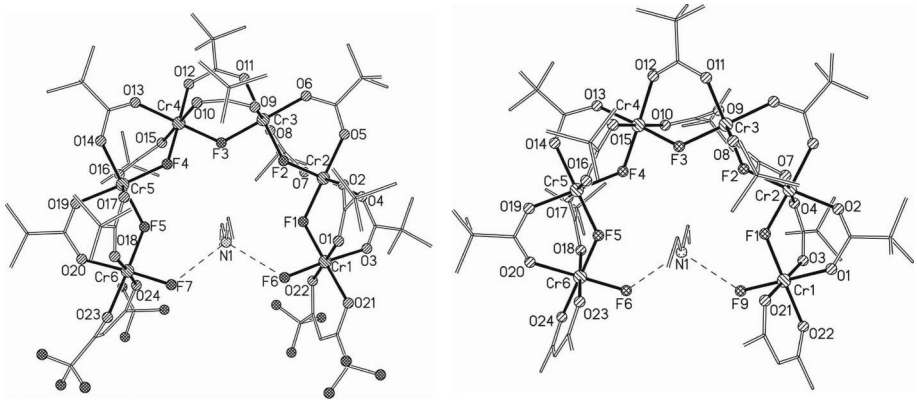

(a) Cr_6hfac **5** (b) Cr_6acac **6**

Fig. 2 (a) Monomeric Cr_6 chain (**5**) terminated at each end with one fluoride and an hfac ligand and (b) Monomeric Cr_6 chain (**6**) terminated at each end with one fluoride and a acac ligand.

pivalic acid. The reaction was then cooled to room temperature and acetone (50 mL) was added and the mixture stirred for 5 h. The resulting solid was collected by filtration, washed with acetone and dried in air. The solid was then extracted with diethyl ether (75 mL), the solution was filtered and evaporated to dryness. The solid was washed with acetone, and dried in air. Yield: 1.7 g (20.2%). Elemental analysis calcd (%) for $C_{156}H_{316}Cr_{14}F_{24}N_6O_{48}$: Cr 17.09, C 43.98, H 7.48, N 1.97; found: Cr 16.83, C 44.31, H 7.71, N 2.13.

4. Compound **2** (0.21 mmol) and 1,1,1,5,5,5-hexafluoro-2,4-pentanedione (Hh-*fac*, 2.10 mmol) were dissolved in CH_2C1_2 (30 mL) and refluxed with stirring for 4 h. The solvent was removed and **4** was isolated by column chromatography on silica gel with 1 : 10 EtOAc–hexane as the eluent; **4** is the first product eluted from the column. Crystals were obtained from EtOAc–CH_3CN (1 : 1) after 1 d (27% yield). Elemental analysis, found: Cr, 16.47; C, 41.02; H, 5.98; N, 0.67%. Calculated for $C_{76}H_{126}Cr_7F_{20}NO_{28}$: Cr, 16.21; C, 40.65; H, 5.66; N, 0.62%.

6. Compound **1** (3.0 g, 0.85 mmol) and Hacac (3.4 g, 3.4 mmol) were dissolved in toluene (200 mL) and the solution refluxed with stirring for 24 h. The solvent was then removed under vacuum, and the resulting solid was washed with MeCN. Compound **6** was isolated by column chromatography on silica gel using THF–*n*-hexane (1 : 2) as eluent. Three fractions resulted, with **6** found in the third fraction. The third fraction was evaporated and washed with MeCN, giving a green microcrystalline solid. Yield: 1.1 g (37.4%). X-Ray quality single crystals were obtained from 1 : 1 Et_2O–MeCN. Elemental analysis calcd (%) for $C_{64}H_{116}Cr_6F_7NO_{24}$: Cr 18.05, C 44.47, H 6.76, N 0.81; found: Cr 17.65, C 43.63, H 6.85, N 0.82.

2.2 X-Ray crystallography

The crystal structures of **4** and **5** have been published previously, and relevant data deposited (CCDC no. 668930 and 725125, respectively).[6,7] Crystal data and data collection and refinement parameters for **6** are given in Table 1. Data were collected on an Oxford Diffraction CCD diffractometer (Mo-Kα, $\lambda = 0.71069$ Å). The selected crystal was mounted on the tip of a glass pin using Paratone-N oil and placed in the cold flow (100 K) produced with an Oxford Cryocooling device. Complete hemispheres of data were collected using ω-scans (0.3°, 30 s per frame). Data collection showed two crystal twins were present which were reduced individually and combined to produce a HKLF5 file. Integrated intensities were obtained with SAINT+[8] and they were corrected for absorption using SADABS.[8] Structure solution and refinement was performed with the SHELX-package.[8] The structures were solved by direct methods and completed by iterative cycles of ΔF syntheses and full-matrix least-squares refinement against F_2. The most disordered pivalate ligands present were modeled using SADI, SAME and EADP restraints. To ensure no NPD's all carbons have been restrained with SIMU and DELU resulting in a large number of restraints (Table 1). Although, there is some residual electron density in cavities it cannot be reliably assigned to any solvents/water.

Table 1 Experimental data for the X-ray study of compound **6**

Formula	$C_{66}H_{119}Cr_6F_7N_2O_{24}$
M	1769.63
Crystal system	Triclinic
Space group	$P\bar{1}$
a/Å	11.8455(5)
b/Å	17.3967(9)
c/Å	24.6928(11)
α/°	100.750(4)
β/°	98.088(4)
γ/°	108.911(4)
U/Å^3	4617.3(4)
T/K	100(2)
Z	2
ρ/g cm^{-1}	1.266
Shape and colour	Green plate
Size/mm	0.8 × 0.4 × 0.1
μ/mm^{-1}	0.757
Unique data	32120
Absorption correction	Multi-scan
Transmission max./min.	0.9281, 0.5825
Ynique data ($F_o > 4\sigma F_o$)	23 612
Parameters/restraints	1042/1919
R_1, wR_2[a]	0.0982, 0.2775
Weighting scheme[b] (w^{-1})	$\sigma^2(F_o^2) + (0.0898P)^2 + 84.9472P$
Goodness of fit	1.102
Largest residuals/e Å^{-3}	1.256, –1.239

[a] R_1 based on observed data, wR_2 on all unique data. [b] $P = 1/3[\max(F_o^2,0) + 2F_c]$.

2.3 Physical measurements

Inelastic neutron scattering experiments on compounds **4** and **6** were performed on the IN5b time of flight inelastic spectrometer[9] at Institute Laue-Langevin, Grenoble, France. The INS spectra collected on 5 were obtained using the FOCUS[10] time of flight spectrometer at the Swiss spallation neutron source SINQ, Paul Scherrer Institute, Villigen, Switzerland. For all INS studies non deuterated, polycrystalline samples were loaded into hollow aluminium cylinders for measurement. The presence of incoherent hydrogen scattering is clearly observed within the spectra, where magnetic features lie on a broad phonon intensity which increases with wave vector transfer and temperature. INS energy spectra were obtained by integration of scattering intensity over all detector angles. Magnetic energy transitions with strong intensity over the background were integrated over the transition energy width to express wave vector transfer dependance. All INS spectra have been detector normalized to vanadium spectra, and background corrected *via* the subtraction of sample environment contributions. A semi empirical Bose subtraction was applied to 5.0 Å energy spectra of **4** and 3.2 Å energy spectra of **6** *via* the subtraction of a temperature re-scaled 60 K measurement; this enabled the removal of the phonon background leaving the spin transitions only for comparison with simulations. Any little remaining background was added to the simulation. EPR at Q-band and W-band frequencies were performed down to 5 K on Bruker EMX and Elexsys spectrometers. Super conducting quantum interference device (SQUID) magnetometry measurements were performed in the temperature range of 1.8–300 K, using a Quantum Design MPMS-XL SQUID magnetometer equipped with a 7 Tesla magnet. Diamagnetic corrections were estimated using Pascal's constants and magnetic measurements were corrected for sample holder contributions.

3 Calculations

Calculations of experimental data have been performed with a microscopic Hamiltonian considering isotropic exchange coupling, and single ion anisotropy where relevant. The coupling of Cr^{3+} ions, total spin 3/2, leads to Hilbert space of 4^6 and 4^7 for the Cr_6 and Cr_7 chains, respectively. The dimensions of the Hamiltonian matrix dimensions have been reduced such that only relevant low lying states are included in the calculation. Such an approach allows for mixing between spin states, due to the presence of anisotropy.

The simulation of the magnetic part of INS spectra has been performed using in-house software based on the Hamiltonian operator given in eqn (1). The Hamiltonian operator describes isotropic exchange coupling between N Cr^{3+} ions with single ion anisotropy. The Heisenberg-Dirac-van-Vleck term is dominant in the Hamiltonian. This term corresponds to nearest neighbour Cr^{3+} spin exchange coupling, where J is a exchange coupling constant and is negative for AF exchange. The second term describes axial ZFS of each Cr^{3+} ion, where D_{Cr} is the axial ZFS parameter. A third term describes single ion rhombic anisotropy, where E_{Cr} is the rhombic ZFS parameter. SQUID and EPR calculations require augmenting the Hamiltonian (1) to include a Zeeman term: $\left(+\sum_i^N \mu_B \mathbf{B}\cdot\tilde{g}\cdot\hat{\mathrm{s}}_{i+1}\right)$;

$$\hat{H} = -J\sum_i^{N-1}\hat{\mathbf{s}}_i\hat{\mathbf{s}}_{i+1} + D_{Cr}\sum_i^N\left(\hat{s}_{z,i}^2 - \frac{1}{3}s_i(s_i+1)\right) + E_{C_r}\sum_i^N\left(\hat{s}_{x,i}^2 - \hat{s}_{y,i}^2\right) \quad (1)$$

Calculations exploit total spin symmetry to reduce numerical and analytical calculation *via* the use of an irreducible tensor operator formalism. The axis for single ion anisotropy is assumed perpendicular to the molecular plane although rotationally site invariant. This means that the calculation of anisotropy does not consider the differences in Cr ion orientation within the molecular plane due to the chains' horseshoe shape. This approximation reduces additional parameterisation and has been sufficient to calculate the INS spectra of similar Cr^{3+} AF rings.[11–13] The mixing of spin states of differing total spin S due to anisotropic interactions is necessary to describe EPR and INS data. A perturbative approach, described in detail previously in Ref. 5 and 14, was adopted for INS calculations, reducing the effective Hamiltonian to include only the states within 10.3 meV of the ground state. This enabled S-mixing within the lowest lying multiplets to be accounted for, while excluding higher lying spin states for reduction of numerical computation. Calculations including a larger number of states were found not to have any effect on the final eigenvalues, and hence the reduced space used is sufficient.

The calculation of the INS transition intensities requires consideration of the interference factor, a description of the interactions between spin centers, the thermal population of the eigenvalues determined by the Hamiltonian operator (1) and the magnetic scattering cross section (providing the transition selection rules $\Delta S = 0, \pm1$ and $\Delta M_S = 0, \pm1$). The interference factor, is dependent on the relative positions of Cr^{3+}, which are known from X-ray crystallography, and spatial properties of the wavefunctions involved in the specific transitions.[15] The magnetic scattering cross section is given by eqn (2),[12] where $A = 0.29$ barn, N is the number of magnetic ions, Z is the partition function, $\mathbf{k}_i$ and $\mathbf{k}_f$ are the initial and final neutron wave vectors, $\mathbf{Q} = \mathbf{k}_i - \mathbf{k}_f$ is the transferred momentum, e^{-2W} is the Debye–Waller factor, E_n is the energy of the n^{th} spin eigenstate, $|n\rangle$. $I_{\text{nm}}(\mathbf{Q})$ is given by eqn (3), where $F_i(Q)$ is the magnetic form factor of the i^{th} spin center, α and β are the Cartesian coordinates of the spin center i and j, $\mathbf{R}_{ij}$ is the position vector between spin centers i and j, $\hat{S}_{i\alpha}$ and $\hat{S}_{i\beta}$ are the local spin operators, and $|n\rangle$ and $|m)$ are the initial and final states of the scattering system respectively. INS experiments were performed on polycrystalline samples, randomising molecular orientation, hence $I_{nm}(\mathbf{Q})$ is averaged over an appropriate number of magnetic scattering vector ($\mathbf{Q}$) orientations, a process explained explicitly in Ref. 15 and demonstrated in Ref. 12

$$\frac{\partial^2\sigma}{\partial\Omega\partial\omega} = \frac{A}{N}\frac{\mathbf{k}_f}{\mathbf{k}_i}e^{-2W}\sum_{n,m}\frac{e^{-\beta E_n}}{Z}I_{nm}(\mathbf{Q})\delta(\hbar\omega - E_m + E_n) \quad (2)$$

$$I_{nm}(\mathbf{Q}) = \sum_{i,j}F_i^*(Q)F_j(Q)e^{i\mathbf{Q}\cdot\mathbf{R}_{i,j}}\sum_{\alpha\beta}\left(\delta_{\alpha\beta} - \frac{Q_\alpha Q_\beta}{Q^2}\right)\times\left\langle n\left|\hat{S}_{i\alpha}\right|m\right\rangle\left\langle m\left|\hat{S}_{j\beta}\right|n\right\rangle \quad (3)$$

We assumed Gaussian line shapes set to the INS instrument resolution. However, in all cases the transition full width half maxima measured are greater than the instrument resolution. This is because of small variations in exchange coupling and anisotropy between chains. Such strain phenomena have been reported previously in heterometallic Cr^{3+} ring complexes, where inclusion of D strain was required to describe EPR spectra,[16] and J strain was required to describe INS spectra.[17] At low energy transfer the shoulders of the elastic line dominate the spectra. The elastic line contribution can be fitted with a Gaussian and a small Lorentzian function. These fits are then added to the simulation of the magnetic band transitions.

SQUID magnetometry calculations were performed using Magnetic Properties Analysis Package for Spin Clusters, MAGPACK.[18] The magnetic behaviour of **4**, **5** and **6** can be described by an isotropic spin Hamiltonian (the first term of Equ. (1) in addition to a Zeeman splitting term for applied magnetic field).

Magnetometry measurements on Cr chains are insensitive to the anisotropic behaviour revealed by INS or EPR and the inclusion of such terms in susceptibility calculations has no significant effect on the calculated curves. EPR simulations were performed *via* a method described in detail previously in references.[16,19] The utilisation of sparse matrix diagonalisation *via* the Davidson algorithm is used to reduce the matrix dimension to include a selection of energetically low lying spin states. Weihe's EPRSIM program[20] was then used to simulate the experimental EPR spectra from the reduced matrix. For the EPR simulation of compound **4**, a reduced matrix dimension to include the first 42 eigenvectors was required.

4 Results and analysis

4.1 Synthesis and structural studies

The discrete single Cr_6 and Cr_7 chains are straightforwardly made from reaction of the dimeric $(Cr_6)_2$ (**1**) and $(Cr_7)_2$ (**2**) horseshoes

Table 2 [a]Bond length (Å) and angle (°) ranges for compounds **4**, **5** and **6**

Compound	**4**	**5**	**6**
Cr–F (bridging)	1.856–1.976	1.902–1.934	1.893–1.945
Cr–O (carboxylate)	1.960–2.041	1.926–1.969	1.943–1.992
Cr–O (diketonate)	2.016–2.096	1.960–1.980	1.930–1.951
Cr–F (terminal)	1.889	1.842	1.864–1.873
O–Cr–O *cis*	85.5–92.3	85.8–97.2	87.5–92.9
O–Cr–O *trans*	178.1–178.4	176.2–179.6	176.3–178.8
O–Cr–F *cis*	88.1–94.1	87.8–93.0	86.5–93.8
O–Cr–F *trans*	175.3–178.5	174.3–179.8	177.3–179.7
F–Cr–F *cis*	87.9–91.5	87.6–90.6	87.4–89.8

[a] Av. Esd = 0.006 Å and 0.2°.

with β-diketonates. Each incoming ligand displaces two terminal fluorides from the horseshoes, and each horseshoe reacts with two ligands with stoichiometry for **5**:

$[(Et_2NH_2)_3Cr_6F_{11}(O_2CtBu)_{10}]_2 + 4Hhfac \rightarrow 2[(Et_2NH_2)Cr_6F_7(O_2CtBu)_{10}(hfac)_2] + 4[Et_2NH_2]F + 4HF$

The single horseshoes are therefore mono-anions, with the charge balanced by an ammonium cation, which is hydrogen-bonded to the centre of the horseshoe (Fig. 2). The six Cr–Cr edges of the horseshoe are all bridged by a single fluoride and two pivalate ligands, while the terminal Cr sites are now bound to a single terminal fluoride and a chelating-diketonate. The result is that a family of finite chains are obtained where the coordination environment at the terminal Cr site is varied without changing the interior of the chain. There are minor structural variations between compounds **4**, **5** and **6**; comparisons of bond length and angle ranges are given in Table 2. The most immediate observation is that there are small number of long Cr–O bond lengths in the structure of compound **4**, and that the single terminal Cr–F bond is also longer than in the hexametallic chains. Comparing the two hexametallic chains, there is a subtle variation at the terminal Cr^{3+} sites; comparing **5** and **6** we find that the Cr–O (diketonate) bonds are shorter in **6** than in **5**, but that the Cr–F (terminal) bonds are longer in **5** than **6**. The differences between **5** and **6** are only just statistically significant.

4.2 Inelastic neutron scattering measurements on 4

INS measurements with a 5.0 Å incident wavelength at temperatures of 1.8, 6.0 and 15.0 K provided access to transitions between the first four spin multiplets. Spectra show high magnetic intensity for a non-deuterated sample. Fig. 3 shows spectra summed over all scattering angles. Fig. 5 shows the spin states accessed by the 5.0 Å measurements of **4** with the observed transitions marked with arrows. Four cold sets of transitions exist, and are labelled **I**, **II**, **III** and **IV** on the neutron energy loss side of the spectrum. **I** corresponds to a transition within the zero field split $S = 3/2$ spin ground state, and can only be resolved at high resolution, see Fig. S11 in the ESI.† Transitions **II** to **IV** all come from the $|\frac{3}{2}\rangle$ ground state and reach up to a $|\frac{1}{2}\rangle$ multiplet (**II**), a $|\frac{5}{2}\rangle$ multiplet (**III**) and energetically close multiplets, $|\frac{3}{2}\rangle$ and $|\frac{1}{2}\rangle$ (**IV**). Splitting present within these total spin transitions shows the presence of significant anisotropy, hence the description of transitions in terms of total S can be considered as an approximate labelling scheme. A broad warm feature labelled **i** corresponds to a transition coming from the first excited $|\frac{1}{2}\rangle$ state at 0.9 meV, reaching the pair excited states $|\frac{3}{2}\rangle$ and $|\frac{1}{2}\rangle$ at around 2.2 meV. Equivalent transitions can

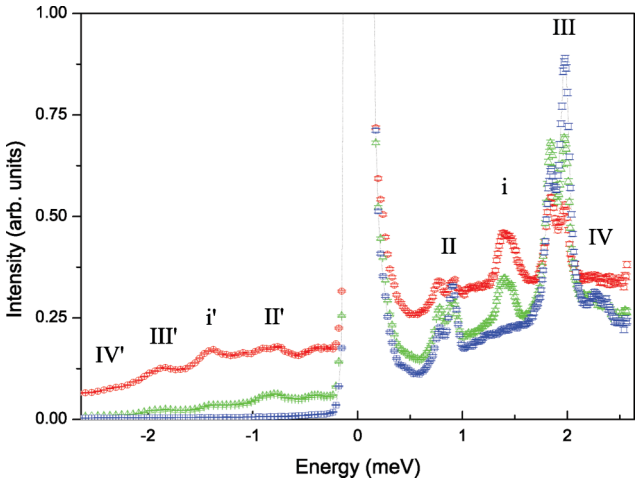

Fig. 3 INS spectra of **4** obtained on IN5 with an incident neutron wavelength of 5.0 Å at 1.8 K (blue open squares), 6.0 K (green open triangles) and 15.0 K (red open circles), summed over all scattering angles. Transition labels are referred to within the text.

be observed in the negative energy transfer domain where **II′**, **i′**, **III′** and **VI′** correspond to the equivalent neutron energy gain transitions observed at 6.0 K and 15.0 K when excited states are thermally populated. The instrumental resolution function of time-of-flight spectrometers is such that resolution in the positive energy transfer domain is greater than in the negative energy domain, hence the focus of analysis described here lies in the positive domain.

INS simulations of **4** for a 5.0 Å incident neutron setting are shown in Fig. 4 with the corresponding experimental data. Calculations lead to the determination of a nearest neighbour Cr^{3+} AF exchange coupling constant of $J = -1.46$ meV ± 0.02, and an axial single ion ZFS of $D_{Cr} = -0.045$ meV ± 0.005. Probing rhombic splitting within spin multiplets in zero field for odd numbered electron system **4**, is not possible due to Kramers degeneracy. Hence for the INS simulation of **4**, the third term in eqn (1) is excluded. Presence of rhombic anisotropy at the Cr sites can be determined with applied magnetic field, and this

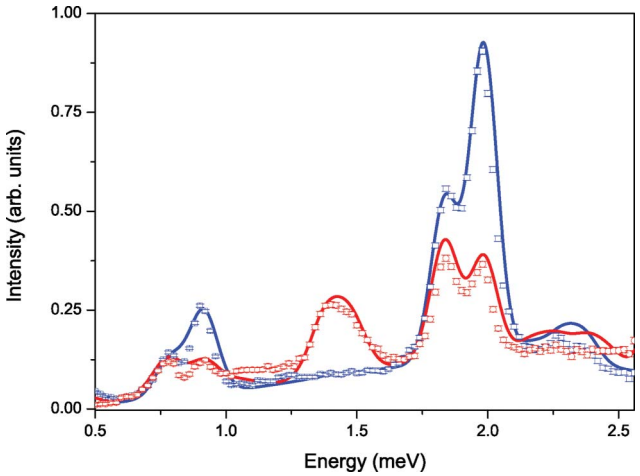

Fig. 4 INS spectra of **4** measured with a 5.0 Å setting after phonon correction for 1.8 K (blue open squares) and 15 K (red open circles). Full lines show simulated spectra with $J = -1.46$ meV and $D_{Cr} = -0.045$ meV.

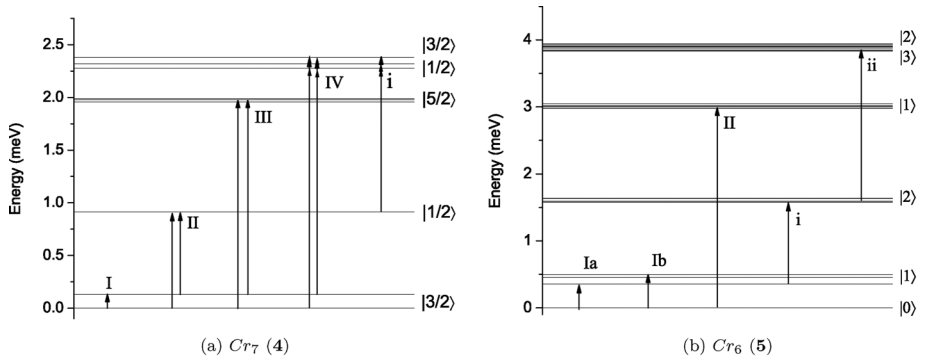

Fig. 5 Calculated eigenvalues for compounds **4** (a) and **5** (b) with observed INS transition labels corresponding to the peaks labelled in Fig. 3 and 6. Eigenvalue spin multiplets are labelled with in their approximate total spin states.

is investigated in the following EPR section. A 9.0 Å incident neutron measurement of **4** enabled the high resolution probing of the ZFS $|\frac{3}{2}\rangle$ ground state for determination of D_{Cr}. Fig. S11 found in the ESI† shows the 9.0 Å 1.8 K spectrum with calculation where $D_{Cr} = -0.045$ meV ± 0.005. A spurious feature is observed, centered at 0.075 meV. This is the result of neutrons scattering incoherently with the sample and sample environment apparatus before reaching the detector. The lack of temperature dependence of this spurious feature confirms its origin as non magnetic. A higher energy transfer setting of incident neutron wavelength 3.2 Å enabled observation of two additional cold transitions at 3.7 and 5.0 meV, see Fig. S12 in the ESI.† Further conformation of the spectroscopic assignments made has been performed by analysis of the Q dependence of specific magnetic band transitions. The calculation of Q dependence intensity for 5.0 Å transitions **i** (centered at 1.42 meV) and **III** (centered at 1.92 meV) have been performed along with inter-multiplet transition **I**, resolved at 9.0 Å Some Q dependence plots with calculations are shown in the ESI, Fig. 13.† The intensity of the 5.0 Å measurement transitions **II** and **IV** were not great enough to determine the Q dependence information over the incoherent background.

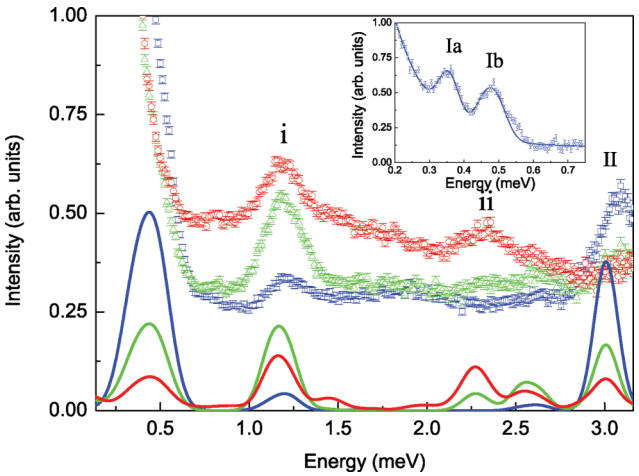

Fig. 6 INS spectra of **5** at 4.4 Å measured at 1.5 K (blue open squares), 6.0 K (green open triangles) and 15.0 K (red open circles). Lines represent calculated spectra, at 1.5 K (solid blue line), 6.0 K (solid green line) and 15.0 K (solid red line). Insert: 6.0 Å spectra of **5** at 1.5 K (blue circles) with a solid blue line representing calculated spectrum. Transition labels are referred to within the text.

4.3 Inelastic neutron scattering measurements on 5 and 6

Fig. 6 shows 4.4 Å incident neutron wavelength measurements on compound **5** with calculated spectra. In these spectra two transitions from the ground state are detected within the experimental energy range, labelled transition **I** and **II**. These transitions have the greatest intensity at 1.8 K confirming that they come from the $|0\rangle$ ground state of the chain. **I** corresponds to a transition reaching the first $|1\rangle$, excited state. **I** is not fully resolved at 4.4 Å and is observed as a shoulder within the elastic line at 1.8 K. **II**, at 3.1 meV, corresponds to a transition reaching the second energetically occurring $|1\rangle$ state. Two warm transitions originating from excited states are observed with differing temperature dependence, transition **i** is most intense at 6 K, while transition **ii** is most intense at 15 K. **i** originates from the first excited $|1\rangle$ state reaching the lowest energy $|2\rangle$ state, while broadened transition **ii** originates from the lowest energy $|2\rangle$ state and accesses additional excited states. A 6 Å measurement at 1.8 K enabled access to transition **I** at high resolution, as shown in the insert of Fig. 6. The labelled transitions **Ia** and **Ib** come from the $|0, 0\rangle$ ground state singlet to the zero field split $|1\rangle$ multiplet. **Ia** reaches the $|1, 0\rangle$ state. **Ib** reaches the $|1, \pm1\rangle$ states and is broadened due to the presence of rhombicity.

The Cr–Cr exchange coupling constant determined for **5** is the same as **4** (see Table 3 for an overview of all the Cr chain physical parameters), suggesting exchange coupling is independent of the chain length. In general the number of incoherently scattered neutrons relative to those magnetically scattered caused Q dependence information to be unobtainable. However for the strongest transition (**i**), centered at 1.2 meV at 6 K, it was possible to determine the general form of the Q dependence. This Q dependence data has been simulated with the same Hamiltonian and parameters, providing further confirmation of the model, see Fig. S14, available in the ESI.† The simulation of the 6.0 Å spectrum determined the axial single ion anisotropy D_{Cr} parameter to be –0.041 meV ± 0.005 and a single ion rhombic anisotropy, $|E_{Cr}|$ of 0.007 meV ± 0.001.

INS measurements of **6** show that the energy level configuration is very similar to **5**, however the differences in transition energies are significant. INS data and simulations of 6.5 and 3.2 Å measurements are available in the ESI (Fig. S15).† The 1.7 K, 3.2 Å measurement gave access to a high energy transfer range,

Table 3 Spin Hamiltonian parameters (meV) for Cr^{3+} finite chains and rings. J_a corresponds to exchange coupling between Cr^{3+} ions terminating the chain. J_b corresponds to nearest neighbour exchange within the body of the chain. Parameterisation is based on the simulation of experimental data as described in the text. Approximate simulation errors are listed with each parameter and are based on the intensity and resolution limitations of the experimental data

Type of chain	J_a	J_b	D_{Cr}	$\lvert E_{Cr} \rvert$
1 $\{Cr_6\}_2$	−1.09 ±0.04	−1.46 ±0.04	−0.028	0.005
2 $\{Cr_7\}_2$	−1.09 ±0.04	−1.46 ±0.04	−0.031	—
3 $\{Cr_8\}$ring[a]	−1.46 ±0.04	−1.46 ±0.04	−0.038 ±0.005	0.004 ±0.001
4 $\{Cr_7\}$hfac	−1.46 ±0.02	−1.46 ±0.02	−0.045 ±0.005	0.007± 0.001
5 $\{Cr_6\}$hfac	−1.46 ±0.04	−1.46 ±0.04	−0.041 ±0.005	0.007 ±0.001
6 $\{Cr_6\}$acac	−1.40 ±0.02	−1.46 ±0.02	−0.045 ±0.005	0.007± 0.001

[a] Values taken from INS study reported in ref. 5.

enabling the identification of an additional S = 1 excited state at 4.7 meV. Calculations performed to simulate INS data from **6** required two separate exchange couplings constants. One exchange constant (J_a) was required to describe exchange between nearest neighbour Cr ions at the ends of the chain, while another constant (J_b) was required to describe exchange between nearest neighbour Cr ions within the body of the chain. J_b, is the same as that determined for compounds **1** to **5**. $J_a = -1.40$ meV, 4% less than J_b.

4.4 Magnetic measurements on 4, 5 and 6

Calculated susceptibility curves for **4**, **5** and **6** use the same exchange coupling parameters as deduced from INS, the details regarding these data and simulations follow in this section. The molecular susceptibility *vs.* temperature of **4** (see Fig. 7) shows a weak increase in susceptibility from 300 to 70 K, where Cr spins are decoupled due to thermal randomisation. At approximately 50 K there is a broad maximum corresponding to AF interactions, and below 20 K susceptibility increases rapidly indicative of the presence of a non diamagnetic ground state. $\chi_M T$ at 300 K equals 11.52 cm^3 K mol^{-1}, which is somewhat smaller than the calculated value for seven uncoupled $\frac{3}{2}$ spins (12.86 cm^3 K mol^{-1}). At low temperature $\chi_M T$ becomes a constant of 1.84 cm^3 K mol^{-1}, consistent with the calculated $\chi_M T$ of a $\frac{3}{2}$ paramagnet. Ref. 7 reported the determination of a nearest neighbour exchange coupling constant of $J = -1.4$ meV for **4** with a Zeeman splitting factor of g = 1.98 determined from susceptibility *vs.* temperature and magnetization *vs.* field. INS enables low lying energy quantum spin levels to be probed directly at a fixed temperature in zero field. Hence INS can be more precise than susceptibility measurements for the determination of exchange coupling parameters. INS results determine a Cr–Cr exchange coupling of −1.46 meV. Susceptibility and magnetization measurements can be calculated to reproduce experimental data with a broad range of parameters; −1.34 to −1.49 meV, while INS measurements enable a single solution to be obtained.

The susceptibility response of **5** (Fig. 7) and **6** (ESI, Fig. S16)† is very similar. In the case of both **5** and **6** χ_M increases as temperature decreases from 300 K. At 20 K a broad inflection, ranging from 40 to 10 K, is observed corresponding to AF interactions. At around 4 K a maximum χ_M value is observed, and as temperature is decreased further from this χ_M decreases rapidly. Calculations reveal that the presence of two maxima corresponds to the topology of the chain. The low temperature maximum is dominated by the coupling of Cr^{3+} ions at the end of the chain, where the terminal Cr^{3+} has only one nearest neighbour. The inflection is dominated by the coupling of Cr^{3+} ions within the body of the chain. The susceptibility maxima for **5** and **6**, occur at the same temperature yet differ slightly in susceptibility. The low temperature maximum (3.5 K) of **6** reaches a susceptibility of 0.138 cm^3 mol^{-1}. The low temperature maximum of **5** reaches a susceptibility of 0.134 cm^3 mol^{-1}. The center of inflection, at 20 K, for **6** is at 0.124 cm^3 mol^{-1}, while for **5** this inflection is at 0.121 cm^3 mol^{-1}. As the temperature approaches 300 K, the susceptibility of **5** and **6** start to deviate again. At 300 K the susceptibility of **6** is 0.035 cm^3 mol^{-1} while **5** is 0.032 cm^3 mol^{-1}. $\chi_M T$ at 300 K equals 10.43 cm^3 K mol^{-1} for **6** and 9.65 cm^3 K mol^{-1} for **5**. $\chi_M T$ at 300 K for both these chains is somewhat less than the calculated susceptibility of 6 uncoupled $\frac{3}{2}$ spins, which is 11.03 cm^3 K mol^{-1}. For **5** a single J model describing nearest neighbour coupling, as for **4**, is the best possible solution to simulate INS and susceptibility data with the calculated curves shown in Fig. 7. The exchange coupling constant, $J = -1.46$ meV, determined from INS gave the best fit across the two experimental techniques. SQUID data can be simulated with a different model adopting two J terms however, with the aid of INS data a one J model was found to be the most accurate parameterisation (further details can be found within the ESI).† The two J model used to describe exchange coupling within **6** was used to calculate the susceptibility for **6**, a Figure of susceptibility data with the calculated curve is given in the ESI.†

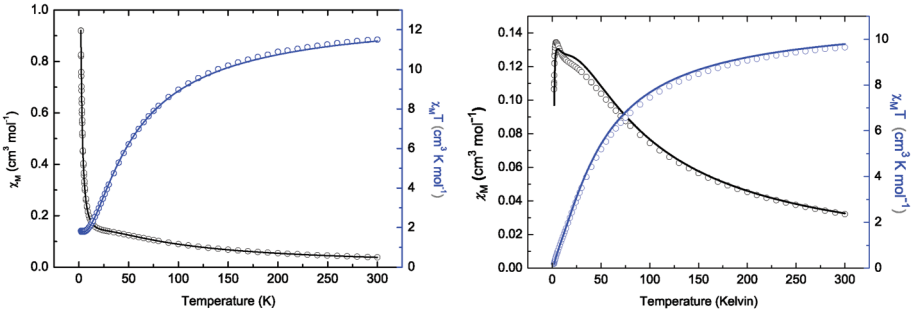

(a) Cr_7 (**4**) (b) Cr_6(**5**)

Fig. 7 Susceptibility *vs.* temperature of **4** and **5**. χ_M *vs.* T, black circles and $\chi_M T$ versus T, blue circles. Solid lines represent calculations, where $g = 1:98$, $J = -1{:}46$ meV for both **4** and **5**.

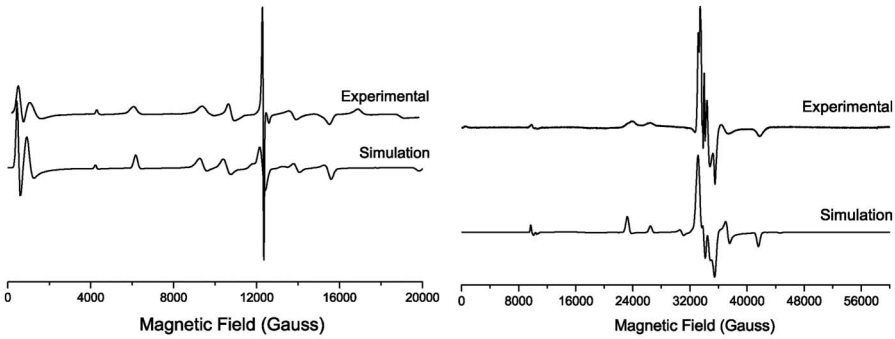

(a) Q-Band spectrum (b) W-band spectrum

Fig. 8 Q-band (34 GHz) and W-band (94 GHz) EPR spectra of **4** at 5 K with simulations including the lowest lying 42 eigenstates, parameters in text.

4.5 EPR measurements on 4

EPR spectroscopy provides information about anisotropic interactions inaccessible by other measurement techniques, due to being highly sensitive to ZFS. Magnetic field swept EPR enables probing of rhombic anisotropy present in **4**. Here we calculate the EPR spectra of **4** using a microscopic Hamiltonian. Single ion anisotropy and isotropic exchange is considered for the calculation of INS spectra. Additionally a rhombic anisotropy parameter is augmented to the Hamiltonian in order to determine the presence of rhombic anisotropy. Fig. 8 shows W-band and Q-band spectra of **4** with calculated spectra. EPR spectral simulations were performed with the spin Hamiltonian parameters determined from INS and magnetometry, *viz.* $J = -1.46$ meV, $g = 1.98$ and axial single ion ZFS of $D_{Cr} = -0.045$ meV, in addition to the determination of the single ion rhombic anisotropy, $|E_{Cr}| = 7\ \mu eV \pm 1$. The simulations correspond with the multi frequency EPR measurements remarkably well considering the simplicity of the Hamiltonian model adopted. Agreement between INS and EPR for the determination of D_{Cr} is exact.

5 Quantitative comparison

The general ordering of states for chains of equivalent length are very similar. Fig. 9 shows the first 12 calculated spin eigenvalues for compounds **1**, **2**, **4** and **5**. Despite such similarities in the general ordering of spin states, the energies and hence exchange coupling between Cr^{3+} ions differ between compounds.

5.1 Structural parameters

The exchange coupling between metal ions is often found to have a strong dependency on ligand angles and distances.[21,22] However, a relationship between the observed differences in exchange coupling for the compounds addressed here can not be clearly explained by structural parameters. In general, the broad statistical range of bond length and angles within compounds make any magneto structural justifications difficult. Table 2 shows there are some subtle variations at the terminal sites comparing **5** and **6**, where Cr–O(diketonate) bond lengths are greater in **5** and Cr–F(terminal) bond lengths are greater in **6**. These differences are only just statistically significant and hence can not be used to correlate differences in J_a exchange measured for the two compounds.

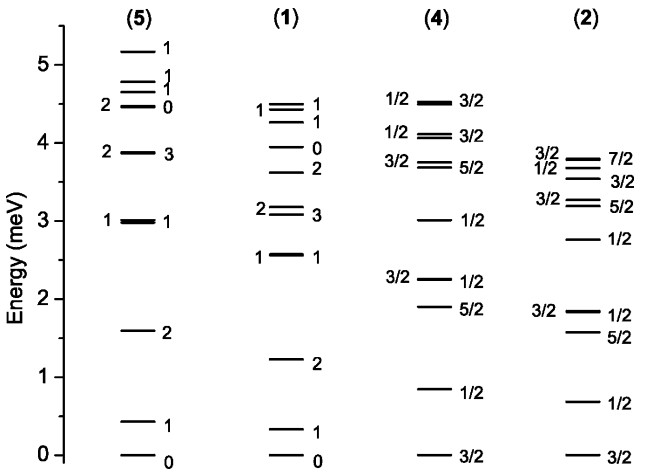

Fig. 9 Energy of the lowest 12 spin Eigenstates for **1** $\{Cr_6\}_2$, **2** $\{Cr_7\}_2$, **4** Cr_7 and **5** (Cr_6). For clarity isotropic exchange is considered only.

5.2 Varying the capping ligand

The homometallic ring **3** and isolated chains **4** and **5** share the same exchange coupling and very similar anisotropy parameters. Isolated chain **6** requires a slightly smaller exchange coupling constant at the end of the chain to simulate INS and SQUID data, while J_b (the Cr–Cr exchange coupling within the body of the chain) is the same as in compounds **3** to **5**. Contrary to the trend that J_b is transferable, physical studies on dimeric chains by Ochsenbein *et al.*[4] reported that seven member chain **2** required quite different exchange coupling constants. **1** was reported to require exchange constants, $J_a = -1.1$ meV and $J_b = -1.4$ meV, coherent with the trend that J_b is equivalent across the whole family. While **2** was modelled with one coupling constant of $J_a = J_b = -1.18$ meV. These findings suggest that J_b for **2** is significantly lower than the other finite chain compounds. Differences in exchange coupling within the body of the chains can not be structurally or electronically explained, hence one would expect J_b to be transferable between chain compounds. Hence, INS and SQUID calculations for **1** and **2**, where J_b is fixed to −1.46 meV, have been performed. In the ESI Fig. S17† shows INS spectra and susceptibility curves for **1**, taken from ref. 4, with calculations where $J_a = -1.09$ meV while $J_b = -1.46$ meV. These parameters are transferable to **2** for the calculation of INS and SQUID data originally reported in ref. 4 The new parameterisation confirms

that Cr–Cr exchange where two nearest neighbour Cr ions exist is equal to −1.46 meV for this class of molecules (compounds: **1** to **6**). Consequently it is the choice of capping ligand only, which effects the spin state composition of the Cr chain, see Fig. 10. In total these end effects are quantified for capping ligands hfac, acac and (F)3 on chains of length six and seven Cr^{3+} ions in length.

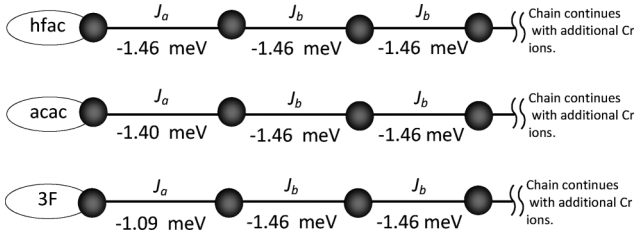

Fig. 10 Schematic diagram to express exchange coupling constants for finite chain compounds **1**, **5** and **6**. Equivalent exchanges for seven membered chains show the same trend in parameterisation.

Substitution of hfac for acac causes the least effect on J_a, where the nearest neighbour atoms coordinated to the terminal Cr ions remain the same as that for Cr ions within the body of the chain. A larger affect is observed with the substitution of $(F)_3$ capping ligands. In this case two of the O atoms coordinated to the terminal Cr ions are exchanged for F ions. A $(F)_3$ capping ligand, leads to a 24% decrease in J_a. An acac capping ligand, leads to a 4% decrease in J_a. The perturbation choice of capping ligand makes on Cr–Cr exchange shows how subtle re-distributions of electron density at a Cr ion site can make a significant measurable effect on exchange coupling. Isolated chains **4** and **5**, show that the effect a hfac ligand has on exchange coupling at the end of the chain is equivalent to two bridging pivalates and a fluoride within the body of a chain. This provides an example of how exchange coupling and anisotropy among these compounds is independent of the inclusion of additional Cr^{3+} ions, from a six to seven member chain, and from a seven member chain to an eight member chain, where the topology is closed into a ring.

5.3 Anisotropy

Considerable anisotropy is present within all the Cr chains. INS studies on polycrystalline samples are only an approximate probe for determination of anisotropy parameters. For this reason calculations have been performed under the approximation that all single ion anisotropy in the molecule is equivalent in magnitude and direction. Dipolar anisotropy interactions between nearest neighbour Cr ions are not negligible, however to reduce parameterisation this effect can be considered to be included within the D_{Cr} parameter. Axial and rhombic anisotropy for **3**, **4**, **5** and **6** are all equivalent, with good confirmation of D_{Cr} and E_{Cr} from multi-frequency EPR for **4**. However, it is most likely that two different axial anisotropy parameters are present for any particular Cr chain, one for Cr ions in the body of the chain and one for Cr ions at the ends of the chain. Additionally, the principal directions of these anisotropies may not lie in the same direction. For this reason chains **1** and **2**, where the capping ligand causes the greatest effect on exchange, have significantly differing parameterisation for D_{Cr} and E_{Cr} than the other chains.

5.4 Conclusion

The Cr horseshoe family can be considered, to a first order approximation, as segments of the Cr_8 (**2**) ring molecule. The availability of such a family of compounds where geometrical variance is limited has enabled an in depth investigation into the effects different capping ligands have on the physical properties of exchange coupling and anisotropy. We have shown that variation of the capping ligand terminating a finite Cr chain has a significant effect on spin state composition and ZFS. Such effects have been quantified by spin Hamiltonian calculations based on INS and SQUID magnetometry data for Cr chains with capping ligands hfac, acac or $(F)_3$. Capping ligands acac and $(F)_3$ terminating six and seven membered Cr chains have been discovered to reduce the magnitude of isotropic exchange coupling by 4% and 24% respectively. Chains with hfac capping ligands show no measurable difference to exchange coupling relative to those within the body of the chain, or equivalently the Cr–Cr exchange coupling present within the Cr_8 (**2**) ring molecule. Varying the terminal ligand presents no clear geometric structural difference around the terminal Cr^{3+} ion, and hence the reason for the observed effects must be electronic. The terminal ligand is shown to affect exchange coupling between Cr ions at the end of the chain, even though it is not a pathway for super exchange. Such a result is clearly relevant for magneto-structural correlations.

There may be some electronic correlation with the Racah inter-electron repulsion parameter B for six coordinate Cr^{3+} complexes with respective capping ligands. B parameters are available for $[CrF_6]^{3-}$, $[Cr(acac)_3]$ and $[Cr(hfacac)_3]$ and are found to be 640,[23] 505 and 383 cm^{-1} respectively, where the free ion B value for Cr^{3+} is 918 cm^{-1} [24] The trend of these B parameters correlates with observed differences in exchange coupling when such ligands terminate the end of a Cr chain. Lower B indicates a larger mean radial displacement of the d shell and smaller mutual interelectronic repulsion. Hence smaller B can refer to the amount of Cr ion electron density that is transferred to the coordinating ligands, this affects the super exchange pathways to the neighbouring Cr ion along the chain. The size of anisotropy present within the Cr chains is an order of magnitude less than that of exchange coupling and in some cases ZFS is on the limit of what can be resolved by INS instruments. To unravel all the details of anisotropy within the chain family, a high frequency EPR study on single crystal samples for several principal molecular orientations will be required. Such a study will be necessary to determine the anisotropy axis for the individual Cr sites, while discriminating local anisotropy at the Cr sites terminating the chain relative to those within the body of the chain.

Acknowledgements

This research project has been supported by the European Commission under the 7th Framework Programme through the 'Research Infrastructures' action of the 'Capacities' Programme, Contract No: CP-CSA INFRA-2008-1.1.1 Number 226507-NMI3. We are grateful to the EC NoE MagMaNet, the EPSRC, and to the Institut Laue-Langevin for funding. REPW is grateful to the Royal Society for a Wolfson Merit Award. We are thankful to Høgni Weihe for the use of EPRSIM and Modesto Clemente for the use of MAGPACK.

References

1 P. W. Anderson, *Phys. Rev.*, 1952, **86**, 694.
2 J. Orenstein and A. J. Millis, *Science*, 2000, **288**, 468.
3 C. F. Hirjibehedin, C. P. Lutz and A. J. Heinrich, *Science*, 2006, **312**, 1021.
4 S. T. Ochsenbein, F. Tuna, M. Rancan, R. S. G. Davies, C. A. Muryn, O. Waldmann, R. Bircher, A. Sieber, G. Carver, H. Mutka, F. Fernandez-Alonso, A. Podlesnyak, L. P. Engelhardt, G. A. Timco, H. U. Güdel and R. E. P. Winpenny, *Chem.–Eur. J.*, 2008, **14**, 5144–5158.
5 S. Carretta, J. van Slageren, T. Guidi, E. Liviotti, C. Mondelli, D. Rovai, A. Cornia, A. L. Dearden, F. Carsughi, M. Affronte, C. D. Frost, R. E. P. Winpenny, D. Gatteschi, G. Amoretti and R. Caciuffo, *Phys. Rev. B: Condens. Matter Mater. Phys.*, 2003, **67**.
6 M. Rancan, G. N. Newton, C. A. Muryn, R. G. Pritchard, G. A. Timco, L. Cronin and R. E. P. Winpenny, *Chem. Commun.*, 2008, 1560–1562.
7 M. L. Baker, M. Rancan, F. Tuna, G. A. Timco, D. Collison, H. Mutka, H.-U. Giidel, R. Pritchard, R. E. Winpenny and E. J. Mclnnes, *Appl. Magn. Reson.*, 2009, **37**, 685–692.
8 *SHELX-PC Package*, Bruker Analytical X-ray Systems, Madison, WI, 1998.
9 J. Ollivier, H. Mutka and L. Didier, *Neutron News*, 2010, **21**, 22.
10 S. Janβen, J. Mesot, L. Holitzner, A. Furrer and R. Hepelmann, *Phys. D*, 1997, **1174**, 234–236.
11 O. Waldmann, T. Guidi, S. Carretta, C. Mondelli and A. L. Dearden, *Phys. Rev. Lett.*, 2003, **91**.
12 R. Caciuffo, T. Guidi, G. Amoretti, S. Carretta, E. Liviotti, P. Santini, C. Mondelli, G. Timco, C. A. Muryn and R. E. P. Winpenny, *Phys. Rev. B: Condens. Matter Mater. Phys.*, 2005, **71**.
13 A. Bianchi, S. Carretta, P. Santini, G. Amoretti, T. Guidi, Y. Qiu, J. R. D. Copley, G. Timco, C. Muryn and R. E. P. Winpenny, *Phys. Rev. B: Condens. Matter Mater. Phys.*, 2009, **79**.
14 E. Liviotti, S. Carretta and G. Amoretti, *J. Chem. Phys.*, 2002, **117**, 3361.
15 O. Waldmann, *Phys. Rev. B: Condens. Matter Mater. Phys.*, 2003, **68**.
16 S. Piligkos, H. Weihe, E. Bill, F. Neese, H. E. Mkami, G. M. Smith, D. Collison, G. Rajaraman, G. A. Timco, R. E. P. Winpenny and E. J. L. Mclnnes, *Chem.–Eur. J.*, 2009.
17 S. Carretta, P. Santini, G. Amoretti, T. Guidi, J. R. D. Copley, Y. Qiu, R. Caciuffo, G. Timco and R. E. P. Winpenny, *Phys. Rev. Lett.*, 2007, **98**.
18 E. C. J. J. Borras-Almenar, J. M. Clemente-Juan and B. S. Tsukerblat, *Inorg. Chem.*, 1999, **38**, 6081–6088.
19 S. Piligkos, E. Bill, D. Collison, E. J. L. Mclnnes, G. A. Timco, H. Weihe, R. E. P. Winpenny and F. Neese, *J. Am. Chem. Soc.*, 2007, **129**, 760–761.
20 J. Glerup and H. Weihe, *Acta Chem. Scand.*, 1991, **45**, 444.
21 H. Weihe and H. U. Güdel, *J. Am. Chem. Soc.*, 1997, **119**, 6539–6543.
22 C. J. Milios, S. Piligkos and E. K. Brechin, *Dalton Trans.*, 2008, 1809.
23 C. K. Jorgenson, *Adv. Chem. Phys.*, **5**, 33.
24 A. B. P. Lever, *Inorganic Electronic Spectroscopy (second edition)*, Elsevier, 1986.

